Theoretical Study of the Alkoxy Radicals Derived from Isoprene: Pressure- and Temperature-Dependent Decomposition Rates

Jiho Park,[†] Joseph C. Stephens,[†] Renyi Zhang,[‡] and Simon W. North*,[†]

Department of Chemistry, Texas A&M University, P.O. Box 30012, College Station, Texas 77842, and Department of Atmospheric Sciences, Texas A&M University, College Station, Texas 77842

Received: March 13, 2003; In Final Form: May 16, 2003

Pressure- and temperature-dependent thermal decomposition rates for the primary alkoxy radicals derived from OH-initiated oxidation of isoprene have been calculated. The master-equation calculations are based on ab initio energetics and structures previously reported. We also provide analytical descriptions of the theoretical falloff curves using the semiempirical Troe formalism. Additional calculations are also provided for two isomers not previously reported and to further characterize basis set effects on the energetics. The results indicate that the decomposition rates for these radicals should not be considered to be in the high-pressure limit at 760 Torr. Under atmospheric conditions the alkoxy radicals will be activated, and we find that prompt reaction for several isomers may be significant. The results are compared to recent estimates of overall alkoxy radical decomposition rates derived from OH cycling studies.

I. Introduction

The tropospheric oxidation of isoprene (2-methyl-1,3-butadiene), initiated primarily by reaction with hydroxyl radicals, has a significant role in ozone production, the long-range transport of NO_x, and regional air quality.[1,2] The reaction between isoprene and the hydroxyl radical proceeds predominately via addition, resulting in four hydroxy radical isomers, two of which are formed in both *E*/*Z* configurations. These radicals subsequently react with ambient O_2 to form hydroxyperoxy radicals. In the presence of moderate NO_x concentrations (>30 ppt), the reaction of the hydroxyperoxy radicals with NO will yield either an organic nitrate or an alkoxy radical and NO_2. The fate of the thermalized alkoxy radicals involves a competition among isomerization, decomposition, and reaction with O_2. The outcome of this competition determines the distribution of first-generation oxidation products which have been quantified previously and includes methyl vinyl ketone (MVK), methacrolien (MACR), formaldehyde, 3-methylfuran, and other minor compounds.[3−13]

There have been several recent theoretical studies on the C−C fission pathways of the alkoxy radicals.[14,15] The decomposition pathways are shown in Figure 1. On the basis of ab initio calculations, Dibble concluded that the barrier to C−C bond cleavage between the α and β carbons is very small (only ∼2 kcal mol^{-1}) in the β-hydroxyalkoxy radicals, indicating that the unimolecular decomposition is the dominant process in these radicals, while the fate of the δ-hydroxyalkoxy radicals involves a competition between isomerization and reaction with O_2.[14] In contrast, Lei and Zhang calculated significantly larger dissociation barriers for the β-hydroxyalkoxy radicals and consequently lower rates although the conclusions of Dibble were unaltered.[15] The difference in barrier heights, however, may have a substantial influence on the role of prompt reactions in these systems and reflects a need to carefully evaluate the theoretical methods employed to study these systems. In this

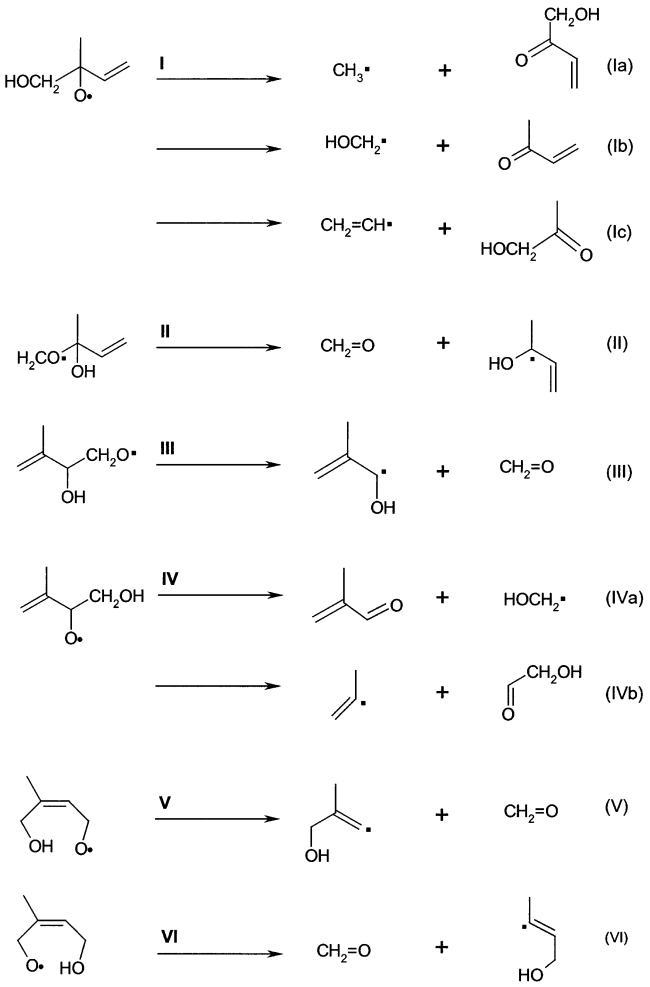

Figure 1. Schematic diagram of the alkoxy radical decomposition channels described in the text.

* To whom correspondence should be addressed. E-mail: swnorth@tamu.edu.
[†] Department of Chemistry.
[‡] Department of Atmospheric Sciences.

10.1021/jp0303321 CCC: $25.00
Published on Web 07/26/2003

TABLE 1: Zero-Point-Corrected Energy Barriers (kcal mol^{-1}) for the Hydroxyisoprene Alkoxy Radical Decomposition Reaction (Pathway Ib)

level of theory	MP2	MP2	MP2	CCSD(T)
basis set	cc-pVDZ	cc-pVTZ	cc-pVQZ	cc-pVDZ
barrier height	14.48	12.58	12.04	8.22

paper we present calculations of the temperature- and pressure-dependent decomposition rates of δ- and β-hydroxyalkoxy radicals derived from isoprene using the master-equation formalism and Rice−Ramsperger−Kassel−Marcus (RRKM) theory based on the ab initio results of Lei and Zhang. Although there have been previous calculations of the high-pressure-limit rate constants using transition-state theory, there is evidence that these systems should not be considered in the high-pressure limit at 760 Torr.[16] We seek to provide more accurate evaluation of the rate constants to incorporate into atmospheric models and to aid in the interpretation of laboratory experiments which are generally performed at low pressures.

In the atmosphere, the hydroxyalkoxy radicals derived from isoprene oxidation are formed by oxygen abstraction from hydroxyperoxy radicals by NO:

$$C_5H_8(OH)O_2 + NO \rightarrow C_5H_8(OH)O + NO_2 \qquad (1)$$

The reaction is exothermic and results in chemically activated hydroxyalkoxy radicals with broad energy distributions that may promptly dissociate or be stabilized through collisions.[17] The fate of these energized radicals and the ratio of prompt decomposition are central to understanding alkoxy reactivity.[18] In this paper we show that prompt decomposition plays an important role and also present results on the thermal decomposition of the stabilized radicals to compare with previous results obtained by transition-state-theory calculations.[14,15] In addition, we provide a comparison between the theoretical predictions and recent OH cycling experiments.[19]

II. Details of Calculation

The barrier heights associated with the decomposition reactions are critical to a quantitative determination of the rates. However, there have been conflicting values reported in the literature.[14,15] We have performed additional ab initio and DFT calculations for pathway Ib to estimate the effects of electron correlation and basis set size on the reaction energetics. The calculations were performed on an SGI Origin 2000 supercomputer using Gaussian 98.[20] Optimized geometries of the alkoxy radical and its transition state were obtained by using Becke's three-parameter hybrid method employing the LYP correction function (B3LYP)[21] in conjunction with the Pople-style split valence polarized basis set 6-31G(d,p). Unscaled B3LYP/6-31G(d,p) vibrational frequencies were used to calculate zero-point corrections. Single-point energy calculations were performed using both second-order Möller−Plesset perturbation theory (MP2) with the frozen core approximation and coupled-cluster theory with single and double excitations including perturbative corrections for the triple excitations (CCSD(T)) with various basis sets.[22,23] The calculated barrier heights shown in Table 1 appear to converge at the CCSD(T) level closer to the value suggested by Lei and Zhang with respect to the basis set size.[24] Therefore, we have elected to use the previous Lei and Zhang values for the barrier heights in the present rate calculations.

We have employed the master-equation formalism to calculate pressure- and temperature-dependent thermal reaction rate constants. The well-defined saddle point along the potential energy surface of the decomposition reactions of hydroxyalkoxy radicals implies that standard RRKM theory can be used to calculate microcanonical rate constants. The RRKM rates are given by the following expression:[25]

$$k(E) = \frac{N^*(E-E_0)}{h\rho(E)} \qquad (2)$$

where $\rho(E)$ is the density of states at the energy E, $N^*(E-E_0)$ is the sum of the states at the transition state, and h is Planck's constant. The rotational constants and vibrational frequencies of the hydroxyalkoxy radicals and their corresponding transition states, along with the energetic barriers for each reaction channel, were obtained from ab initio calculations previously reported by Lei and Zhang.[14] Internal rotations were treated in the harmonic approximation. The density and sum of states were obtained through a direct count procedure by the Beyer−Swinehart algorithm[26] with an energy increment of 1 cm^{-1}. Unscaled vibrational frequencies and moments of inertia required to evaluate the microscopic rate coefficient $k(E)$ were taken from recent ab initio calculations. The external rotations were treated assuming that the molecules were symmetric tops with external rotation about the smallest moment of inertia active and the two remaining external rotations considered adiabatic. There was no reaction path degeneracy for the decomposition reactions considered.

The transformation from the microcanonical rates to thermal rate constants involves the master-equation formalism, which includes both activation and deactivation processes. The time-dependent energy-grained master equation can be expressed as[25]

$$\frac{dn_i}{dt} = Rf_i + \omega\sum_j P_{ij}n_j - \omega n_i - k_i n_i \qquad (3)$$

where n_i is the concentration of the system of interest at the ith energy state, R is the formation rate, f_i is the initial distribution probability, ω is the collision frequency with bath gas, P_{ij} is the transition probability from the jth energy state to the ith energy state, and k_i is the unimolecular reaction rate. The first two terms in the equation represent population from the reactant or other energy states, and the last two terms represent depopulation to either products or other energy states. Small monatomic or homonuclear diatomic colliders such as N_2, which is the most abundant species in the atmosphere, are not amenable to the strong collision approximation, and we have performed all calculations in the framework of a weak collision model by applying the exponential down model. We have adopted $\Delta E = 200$ cm^{-1} as the energy-transfer parameter for all temperatures studied, close to the values previously used for similar systems.[16,27,28] There is no substantial experimental evidence that ΔE should vary significantly with temperature.[29−31] Recent calculations on C_2-C_5 alkoxy radicals using the biased random walk method showed only small variation over the temperature range of the present studies.[16] We find only small differences between falloff curves calculated using $\Delta E = 300$ cm^{-1}, certainly within the variation due to other sources of error.

The solution of the master equation constitutes an integral eigenvalue problem from which the thermal rate constants at a given pressure and temperature can be obtained from the smallest negative eigenvalue. In the case of a single channel reaction the smallest negative eigenvalue can be directly identified as the thermal rate constant. Although multiple channels can be treated independently in the high-pressure limit, this is not true in the falloff region where channels compete at each microcanonical energy and the populations of the highest

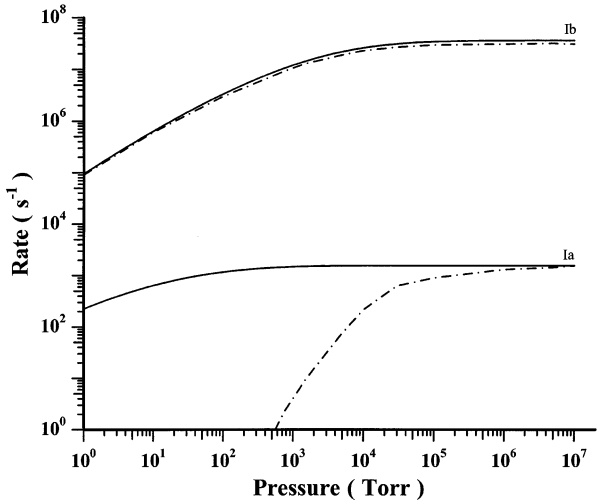

Figure 2. RRKM/ME falloff curves for pathways Ia and Ib using a single-channel model (solid lines) and a multichannel model (dashed lines).

energies are depleted by the lowest threshold reactions. The MULTIWELL multiple-channel method, which uses a stochastic method rather than an eigenvalue method, was used for the decomposition of isomer **I** through pathways Ia and Ib at 298 K, and the results are shown as dashed lines in Figure 2.[32] For comparison the falloff curves predicted by treating the channels as decoupled are shown as solid lines. Even at ambient pressure there is a substantial suppression of the higher barrier pathway (Ia). On the basis of this behavior, one needs only to consider the falloff curves for the lower barrier pathways to describe the alkoxy decomposition behavior for each isomer, since the predicted curves for the independent channel model proved a reasonable description of the lowest barrier channel. We have calculated the collision frequency on the basis of a Lennard-Jones interaction potential for which the appropriate value is given by the standard hard-sphere collision frequency multiplied by the reduced collision integral. The necessary quantities for the self-collisions of many bath gases (e.g., N_2) and several reactant molecules are listed in the literature.[33] In the case of the hydroxyalkoxy radicals it is necessary to estimate ϵ and σ since these are not available. We calculated their values using empirical formulas[33] and include averaging between the different collision partners. The values of $\epsilon = 152.7$ K and $\sigma = 4.99$ Å have been adopted as Lennard-Jones parameters for the current study.

All rate constant calculations were performed in the temperature range of 220−310 K, appropriate for the conditions found in the troposphere. To ensure that the low- and high-pressure-limiting regions were encompassed, the pressure was varied from 1 to 10^7 Torr. We have also solved the master equation for sufficiently small pressure intervals to accurately model the falloff curves. The semiempirical Troe formalism[34] is widely used among atmospheric scientists to describe the falloff behavior. The expression of this form is given by

$$k([\mathrm{M}],T) = \frac{k_0(T)[\mathrm{M}]}{1 + k_0(T)[\mathrm{M}]/k_\infty(T)} F^{(1+(\log(k_0(T)[\mathrm{M}]/k_\infty(T)))^2)^{-1}} \quad (4)$$

where [M] is the concentration of the buffer gas, $k_0(T)$ is the low-pressure termolecular rate constant, $k_\infty(T)$ is the high-pressure-limiting rate constant, and F is the collision-broadening factor. The high-pressure-limiting rate constants were directly obtained from RRKM/ME calculation, and $k_0(T)$ and F were varied to obtain the best fit to the RRKM/ME falloff curves by the nonlinear square fitting method. We find that all falloff curves for the lowest barrier channels can be modeled with a temperature-independent value of $F = 0.4$, which is lower than $F = 0.6$ recommended for atmospheric modeling.[35] It should be noted that recent work by Somnitz and Zellner reported similar values for the decomposition of C_4 and C_5 alkoxy radicals.[16]

TABLE 2: Zero-Point-Corrected Energy Barriers (kcal mol^{-1}) for the Hydroxyisoprene Alkoxy Radical Decomposition Reaction (Isomers V and VI)

isomer	B3LYP/ 6-31G(d,p)	MP2/ 6-31G(d)	MP2/ 6-3111G(d,p)	CCSD(T)/ 6-31G(d)	CCSD(T)/ 6-31G(d)+CF
(*Z*)-**V**	22.49	26.53	24.72	22.68	20.87
(*E*)-**V**	24.15	34.10	31.77	25.74	23.41
(*Z*)-**VI**	17.77	22.78	21.16	19.50	17.88
(*E*)-**VI**	18.77	30.63	28.52	22.70	20.59

III. Results and Discussion

Thermal Decomposition Rates. A schematic diagram of the hydroxyalkoxy radical decomposition pathways is shown in Figure 1. We have included only the *Z* configurations of isomers **V** and **VI** since the decomposition products are identical.[36] Table 2 shows ab initio calculations of the barrier heights for the *E* configurations, which have not been previously reported. We find that although the barrier heights are similar to those associated with the *Z* configurations, they are slightly higher. According to a previous study[37] there should be substantial variation in the relative branching ratios of the hydroxyperoxy radical isomers which should map onto the relative yields for the hydroxyalkoxy radical isomers. The origin of this branching is the strong preference for OH addition to the outer carbons of isoprene.[38] In particular, the isomers **I**, **IV**, and **V** are predicted to be formed in significant fractions of 0.34, 0.29, and 0.22, respectively. Isomers **II** and **III**, which result from initial OH addition to the inner positions of isoprene, are formed in minor fractional yield (0.02 and 0.05). It should be noted that this result is in contrast to the model of Paulson and Steinfeld that assigns comparable weights to all the peroxy radical isomers.[12] The fate of the hydroxyalkoxy radical reactions involves three pathways, decomposition, isomerization, and the hydrogen abstraction reaction with O_2. The recommended rates of isomerization and hydrogen abstraction reaction under ambient conditions are 10^6 and 4×10^4 s^{-1}, respectively.[39,40] Although the isomerization rate is strongly dependent on the structure of the alkoxy radical, the rate of O_2 reaction is not thought to vary significantly. The hydroxy functionalization is not thought to have a pronounced effect.[41]

There are three possible reaction pathways for the decomposition of isomer **I** which have been identified previously.[14] Pathway Ic, the endoergic loss of vinyl radical, has a relatively high barrier height of 22.4 kcal mol^{-1} and as a consequence will be relatively unimportant. The falloff curves calculated between 1 and 10^7 Torr for pathway Ib over the temperature range 220−310 K are shown in Figure 3. We find that pathway 1b is strongly favored and, therefore, consider only pathway Ib, yielding methoxy radicals and methyl vinyl ketone, which will be the dominant decomposition pathway under all conditions considered. Since there is no facile isomerization or hydrogen atom abstraction reactions for isomer **I**, decomposition will be the sole fate of thermalized radicals. Even at very low pressures and high temperatures the preference for pathway Ib over pathway Ia is more than an order of magnitude. The calculations also show that at 300 K and 760 Torr the rate for

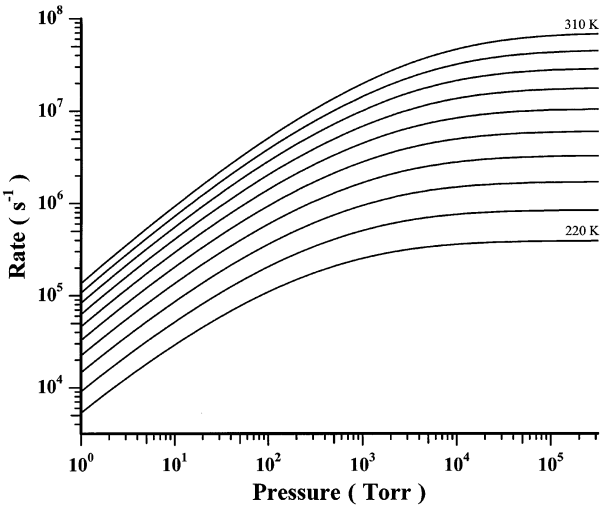

Figure 3. RRKM/ME falloff curves for the decomposition of isomer **I** via pathway 1b over the temperature range 220−310 K in increments of $\Delta T = 10$ K. The bath gas for all curves is N_2.

TABLE 3: Decomposition of Alkoxy Radical I via Pathway Ib[a]

pressure (Torr)	barrier height (kcal/mol)	activation energy (kcal/mol)	k(220 K)	k(300 K)
$\rightarrow\infty$	7.2	7.79	3.90×10^5	4.48×10^7
760	7.2	6.46	2.33×10^5	1.23×10^7
200	7.2	6.01	1.50×10^5	6.06×10^6
$\rightarrow 0$	7.2	5.28	1.83×10^{-13}	4.81×10^{-12}

[a] Rates are in s^{-1} except the low-pressure-limit rate, which is in cm^3 $molecules^{-1}$ s^{-1}.

pathway Ib is 1.2×10^7 s^{-1}, 70% lower than the high-pressure-limit rate constant calculated using TST. The activation energy and preexponential factor for pathway Ib were also determined and are summarized in Table 3.

Isomers **II** and **III** each decompose through a single pathway, producing formaldehyde and a hydroxyalkyl radical in both cases. The barrier heights for both processes are small, and the reactions are very exothermic due to the weak C−C bond energy. The transition-state-theory rate constants for the decomposition of isomers **II** and **III** of 1.3×10^8 and 6.0×10^8 s^{-1} reported by Lei and Zhang are in good agreement with our high-pressure-limit values calculated to be 1.2×10^8 and 5.2×10^8 s^{-1} at 300 K. Both radicals exhibit falloff behavior starting at $\sim 10^4$ Torr, and it should be noted that the rates at 760 Torr are almost an order of magnitude lower than the high-pressure limit values. Figures 4 and 5 show pressure and temperature dependence of the decomposition rates for isomers **II** and **III**. High- and low-pressure-limit rate constants as well as the rates at tropospheric conditions are given in Tables 4 and 5. Isomer **II** has no facile isomerization pathway, so decomposition will be the dominant fate. Although isomer **III** does have a 1,5 hydrogen shift pathway, the rate is estimated to range from 3×10^3 to 5×10^5 s^{-1} depending on the ab initio method used to calculate the barrier height.[36] Since both values for the isomerization rate are significantly smaller than the decomposition rates, the latter will still dominate.

Isomer **IV** is formed in a high fraction (0.29) and has two different decomposition pathways. One of the pathways (IVa) is facile, breaking the weakly bonded C−C bond, producing hydroxymethyl radical and methacrolein. The high-pressure rate of the reaction is determined to be 2.8×10^8 s^{-1} at 300 K (Figure 6 and Table 6). The decomposition exhibits a strong pressure dependence and is already in the falloff region at 760 Torr. The value of the rate constant at 300 K and 760 Torr is almost a factor of 5 lower than the high-pressure limit. The other reaction pathway (IVb) has a large barrier height and will play a negligible role. Since there is no facile isomerization pathway for isomer **IV**, decomposition will be the dominant fate.

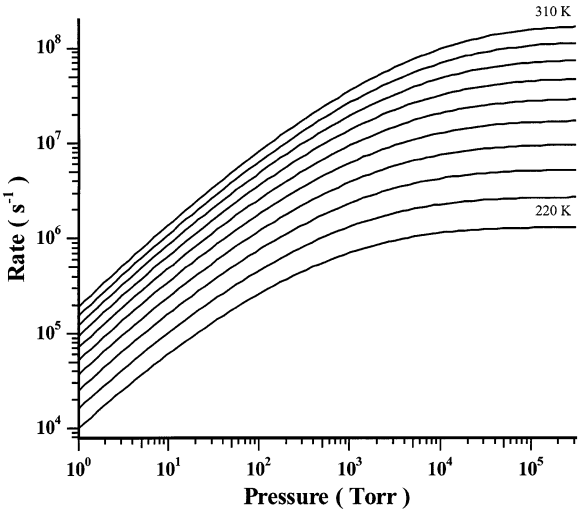

Figure 4. RRKM/ME falloff curves for the decomposition of isomer **II** over the temperature range 220−310 K in increments of $\Delta T = 10$ K. The bath gas for all curves is N_2.

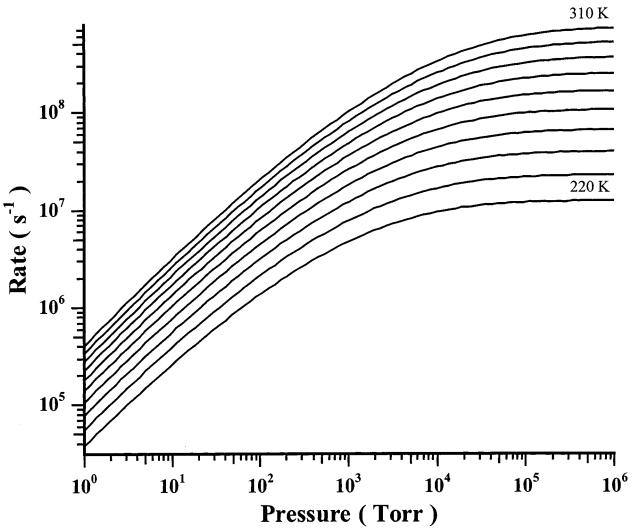

Figure 5. RRKM/ME falloff curves for the decomposition of isomer **III** over the temperature range 220−310 K in increments of $\Delta T = 10$ K. The bath gas for all curves is N_2.

TABLE 4: Decomposition of Alkoxy Radical II[a]

pressure (Torr)	barrier height (kcal/mol)	activation energy (kcal/mol)	k(220 K)	k(300 K)
$\rightarrow\infty$	6.7	7.34	1.32×10^6	1.16×10^8
760	6.7	5.79	6.37×10^5	2.25×10^7
200	6.7	5.38	3.73×10^5	1.03×10^7
$\rightarrow 0$	6.7	4.46	3.13×10^{-13}	4.59×10^{-12}

[a] Rates are in s^{-1} except the low-pressure-limit rate, which is in cm^3 $molecules^{-1}$ s^{-1}.

Isomers **V** and **VI** each have *E* and *Z* configurations, only the *Z* configurations of which are shown in Figure 1. The barrier heights associated with decomposition for the *E* and *Z* configurations of both isomers are very large, and the high-pressure rates of decomposition are 3.4×10^{-3} and 6.0×10^{-1} s^{-1} for the reactions of **V** and **VI**, respectively. The results suggest that

TABLE 5: Decomposition of Alkoxy Radical III[a]

pressure (Torr)	barrier height (kcal/mol)	activation energy (kcal/mol)	k(220 K)	k(300 K)
$\rightarrow\infty$	5.6	6.14	1.24×10^{7}	5.23×10^{8}
760	5.6	4.52	4.14×10^{6}	6.71×10^{7}
200	5.6	4.21	2.11×10^{6}	2.83×10^{7}
$\rightarrow 0$	5.6	3.83	9.05×10^{-13}	9.36×10^{-12}

[a] Rates are in s^{-1} except the low-pressure-limit rate, which is in cm^3 $molecules^{-1}$ s^{-1}.

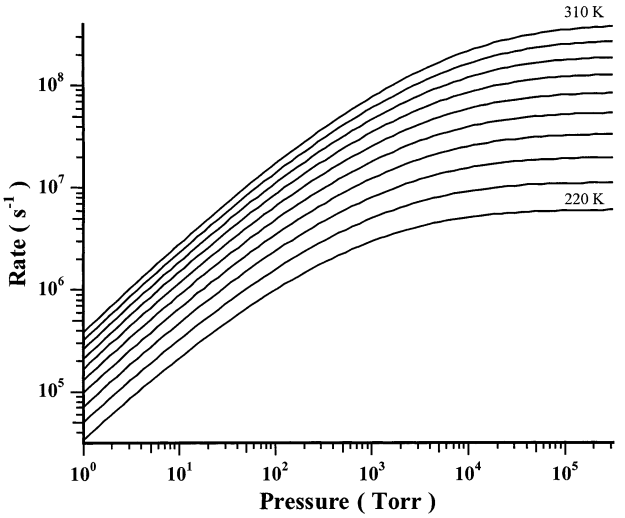

Figure 6. RRKM/ME falloff curves for the decomposition of isomer **IV** via pathway IVa over the temperature range 220−310 K in increments of $\Delta T = 10$ K. The bath gas for all curves is N_2.

TABLE 6: Decomposition of Alkoxy Radical IV via Pathway IVa[a]

pressure (Torr)	barrier height (kcal/mol)	activation energy (kcal/mol)	k(220 K)	k(300 K)
$\rightarrow\infty$	5.8	6.26	6.07×10^{6}	2.75×10^{8}
760	5.8	4.79	2.65×10^{6}	5.06×10^{7}
200	5.8	4.43	1.47×10^{6}	2.26×10^{7}
$\rightarrow 0$	5.8	3.88	8.35×10^{-13}	8.91×10^{-12}

[a] Rates are in s^{-1} except the low-pressure-limit rate, which is in cm^3 $molecules^{-1}$ s^{-1}.

decomposition will be unimportant relative to either O_2 reaction and isomerization. The Z configurations of isomers **V** and **VI** shown in Figure 1 have been shown to have isomerization rates of 8.5×10^{7} and 1×10^{8} s^{-1} under ambient conditions, significantly faster than reaction with O_2.[40,36] However, the E configurations exhibit slower isomerization, particularly the (*E*)-**VI** isomer, which requires a 1,4 hydrogen shift over a large barrier, and for these species O_2 reaction may still play an important role.

Prompt vs Thermal Decomposition. In the previous section we evaluated the pressure- and temperature-dependent decomposition rates for thermalized alkoxy radicals. However, the nascent alkoxy radicals, formed from the $RO_2 + NO$ reaction, are highly activated. There have been previous theoretical investigations of the reaction of peroxy radicals with NO. Tyndall and co-workers discussed the role of prompt alkoxy radical decomposition in the oxidation of HFC-134a on the basis of experimental observations.[42] There have since been several studies employing RRKM/ME formalism for a number of small alkylperoxy radicals, notably, the peroxy radicals formed from the oxidation of propene and ethene.[43−45] We have recently performed calculations of the fate of the hydroxyperoxy nitrites derived from isoprene oxidation using the steady-state master-equation (ME) formalism in conjunction with the variational-RRKM method.[17] Although a determination of the branching between nitrate formation and $RO + NO_2$ channels is problematic, the minor nitrate yield has little effect on the nascent energy distribution of the alkoxy radicals. The initial and steady-state energy distributions of isomer **I** as well as the microcanonical reaction rates are shown in Figure 7. Details of the calculations have been described elsewhere.[17] If the system reaches steady state, the number density at a specific energy is time independent, and eq 3 can be expressed as

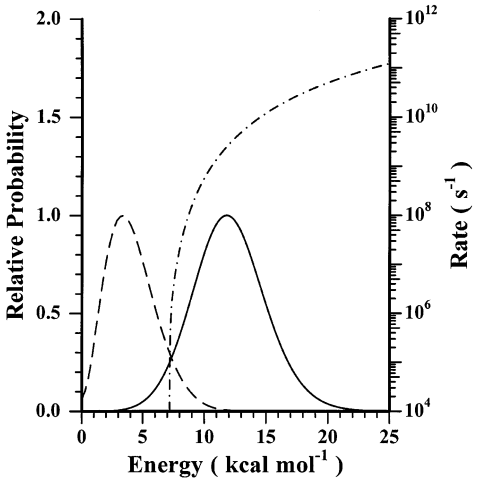

Figure 7. Initial (—) and steady-state (---) energy distributions of isomer **I** at 760 Torr and 295 K. The microcanonical reaction rate (-•-) is also shown.

TABLE 7: Fraction of Prompt Reaction in Hydroxyisoprene Alkoxy Radical Decomposition[a]

pressure (Torr)	pathway Ia	pathway Ib	pathway II	pathway III	pathway IVa
1	0.15	0.96	0.98	1.00	0.99
3	0.11	0.95	0.97	0.99	0.99
10	0.07	0.93	0.97	0.99	0.98
100	0.02	0.85	0.92	0.98	0.95
760	0.00	0.68	0.82	0.94	0.86

[a] For pathways Ic, IVb, V, and VI, the prompt ratio is less than 0.01 and the data are not shown.

$$R\mathbf{F} = K\mathbf{N} + \omega(\mathbf{I}-\mathbf{P})\mathbf{N} \tag{5}$$

where **F** is the matrix representation of the initial energy distribution, **I** is the unit matrix, **P** is the matrix representation of the transition probability, and **N** is the matrix representation of the steady-state concentration of the system.[25] Although the majority of the steady-state energy distribution of alkoxy radical isomer **I** lies below the energetic threshold, the fraction of prompt reaction is given by the ratio of the output flux above the barrier and constant input flux:

$$\frac{\sum_i (K\mathbf{N})_i}{R} = \sum_i (KX^{-1}\mathbf{F})_i \tag{6}$$

where $X = K + \omega(\mathbf{I}-\mathbf{P})$. The calculated fractions of prompt reaction as a function of pressure at 295 K are shown in Table 7. Even under atmospheric conditions, the prompt reaction ratios for isomer **I** through pathway Ib and isomer **IV** through pathway IVa were determined to be 0.68 and 0.86, respectively. Our calculations suggest that, for the β-hydroxyalkoxy radicals (isomers **I**, **II**, **III**, and **IV**), prompt decomposition is significant.

The ratio of prompt reaction to thermalization increases as the pressure decreases in accordance with less collisional deactivation at lower pressure. In contrast, decomposition of the δ-hydroxyalkoxy radicals (isomers **V** and **VI**) which possess relatively high reaction barriers is negligible. For pathways Ic, IVb, V, and VI, the prompt reaction ratio is less than 0.01 and the data are not shown. Recent studies show that prompt isomerization of δ-hydroxyalkoxy radicals through 1,5 H-shift is the dominant reaction pathway.[36,40]

Comparison with Recent Experiments. The pressure dependence of the hydroxyalkoxy decomposition rates has important implications for interpreting laboratory experiments which are often performed at lower pressures than ambient. Recently, Reitz et al.[19] reported an overall hydroxyalkoxy radical decomposition rate of $(3.0 \pm 0.5) \times 10^4$ s^{-1} at 3−4 Torr and 295 K which was 3 orders of magnitude slower than the high-pressure-limited rate constants calculated using transition-state theory by Lei and Zhang for isomers **I**−**IV**.[15] The calculated pressure-dependent rate constant curves indicate that the decomposition rates for these isomers are in the falloff region even under ambient tropospheric conditions and that the rates at 3−4 Torr should be significantly lower than predicted from transition-state theory. We predict rate constants of 2.4×10^5 and 7.8×10^5 s^{-1} for pathways Ib and Iva, respectively, at 3 Torr and 295 K. These rate constants are about an order of magnitude larger than the averaged value derived from the cycling experiment. Isomers **V** and **VI** are predicted to be formed in a 0.30 fractional yield.[37] Although isomers (*E*)- and (*Z*)-**V** and (*E*)-**VI** undergo isomerization, the isomerization products still contribute to OH regeneration. Dibble[36] has suggested that the resulting dihydroxy radicals either react with O_2 to produce HO_2 directly or react successively with O_2 and NO to form dihydroxyalkoxy radicals. Dihydroxyalkoxy radicals are precursors of HO_2 in the presence of O_2 and NO. In both cases, further reaction of HO_2 with NO will produce hydroxyl radical. The branching ratios of those reactions have not yet been accurately quantified. However, considering reported rates of $\sim 10^{-12}$ cm^3 molecule^{-1} s^{-1} for alkyl radical reactions with O_2,[46] and rates of $> 10^{-11}$ cm^3 molecule^{-1} s^{-1} for α-hydroxyalkyl radical reactions with O_2,[47] the latter pathway (hydrogen abstraction) is likely dominant. The *Z* configuration of isomer **VI**, which does not have a labile hydrogen, would serve as a minor hydroxyl radical sink on the time scale of previous experiments.

It should be noted that the decomposition rate constants described above were calculated assuming initially thermalized alkoxy radicals. The authors of the previous experimental studies[19] reported that the fraction of prompt alkoxy decomposition should be minor. This is inconsistent with the large contribution of prompt alkoxy decomposition shown in Table 7. The estimation of the prompt fragments, however, is strongly dependent on the alkoxy barrier heights and the RRKM/master-equation treatment and energetics of the RO_2 + NO reaction. For example, an increase in barrier height for pathway Ib by 2 kcal mol^{-1} reduces the prompt reaction ratio from 0.68 to 0.23 at 760 Torr and 295 K. Calculation of the nascent alkoxy energy distribution also depends on the accuracy of the SSE method of predicting the energy partitioning. To resolve this discrepancy between experiment and theory, it will be necessary to perform the experiment under conditions which are more sensitive to the decomposition rates and as a function of temperature.

IV. Conclusions

We have calculated pressure- and temperature-dependent decomposition reaction rates for the hydroxyalkoxy radicals derived from the OH-initiated oxidation of isoprene. We find that the decomposition reaction rates for the β-hydroxyalkoxy radical lie in the falloff region even at atmospheric pressure and room temperature, and hence high-pressure-limit rate constants are not valid for simulations under atmospheric conditions. The prompt reaction fractions of alkoxy radicals were determined and suggest that the rapid decomposition of energized radicals may play an important role.

Acknowledgment. We acknowledge extensive conversations with Dr. Theodore Dibble. This work was supported by the Texas Advanced Research Program (Grant No. 010366-0306) and the National Science Foundation (Grant No. CHE-0204705). Work by J.C.S. was supported by the National Science Foundation REU program (Grant No. CHE-0071889). We thank Dr. W. Sean McGivern for valuable assistance.

Supporting Information Available: Frequencies and moments of inertia of all species calculated by using Becke's three-parameter hybrid method employing the LYP correction function (B3LYP) in conjunction with the Pople-style split valence polarized basis set 6-31G(d,p). This material is available free of charge via the Internet at http://pubs.acs.org.

References and Notes

(1) Rasmussen, R. A.; Khalil, M. A. *J. Geophys. Res.* **1988**, *93*, 1417.

(2) Trainer, M.; Williams, E. J.; Parrish, D. D.; Buhr, M. P.; Allwine, E. J.; Westberg, H. H.; Fehsenfeld, F. C.; Liu, S. C. *Nature* **1987**, *329*, 705.

(3) Lloyd, A. C.; Atkinson, R.; Lurmann, F. W.; Nitta, B. *Atmos. Environ.* **1983**, *17*, 1931.

(4) Killus, J. P.; Whitten, G. Z. *Environ. Sci. Technol.* **1984**, *18*, 142.

(5) Arnts, R. R.; Gay, B. W., Jr. *Photochemistry of Some Naturally Emitted Hydrocarbons*; EPA-600/3-79-081; U.S. Environmental Protection Agency: Washington, DC, 1979.

(6) Atkinson, R.; Aschmann, S. M.; Tuazon, E. C.; Arey, J.; Zielinska, B. *Int. J. Chem. Kinet.* **1989**, *21*, 593.

(7) Gu, C. I.; Rynard, C. M.; Hendry, D. G.; Mill, T. *Environ. Sci. Technol.* **1985**, *19*, 151.

(8) Tuazon, E. C.; Atkinson, R. *Int. J. Chem. Kinet.* **1990**, *22*, 1221.

(9) Paulson, S. E.; Flagan, R. C.; Seinfeld, J. H. *Int. J. Chem. Kinet.* **1992**, *24*, 79.

(10) Grosjean, D.; Williams, E. L., II; Grosjean, E. *Environ. Sci. Technol.* **1993**, *27*, 830.

(11) Kwok, E. S.; Atkinson, R.; Arey, J. *Environ. Sci. Technol.* **1995**, *29*, 2467.

(12) Paulson, S. E.; Seinfeld, J. H. *J. Geophys. Res.* **1992**, *97*, 20703.

(13) Sprengnether, M.; Demerjian, K. L.; Donahue, N. M.; Anderson, J. G. *J. Geophys. Res.* **2002**, *107*, 4269.

(14) Dibble, T. S. *J. Phys. Chem. A* **1999**, *103*, 8559.

(15) Lei, W.; Zhang, R. *J. Phys. Chem. A* **2001**, *105*, 3808.

(16) Somnitz, H.; Zellner, R. *Phys. Chem. Chem. Phys.* **2000**, *2*, 1907.

(17) Zhang, D.; Zhang, R.; Park, J.; North, S. W. *J. Am. Chem. Soc.* **2002**, *124*, 9600.

(18) Wallington, T. J.; Hurley, M. D.; Fracheboud, J. M.; Orlando, J. J.; Tyndall, G. S.; Sehested, J.; Mogelberg, T. E.; Nielsen, O. J. *J. Phys. Chem.* **1996**, *100*, 18116.

(19) Reitz, J. E.; McGivern, W. S.; Church, M. C.; Wilson, M. D.; North, S. W. *Int. J. Chem. Kinet.* **2002**, *34*, 255.

(20) Frisch, M. J.; Trucks, G. W.; Schlegel, H. B.; Scuseria, G. E.; Robb, M. A.; Cheeseman, J. R.; Zakrzewski, V. G.; Montgomery, J. A., Jr.; Stratmann, R. E.; Burant, J. C.; Dapprich, S.; Millam, J. M.; Daniels, A. D.; Kudin, K. N.; Strain, M. C.; Farkas, O.; Tomasi, J.; Barone, V.; Cossi, M.; Cammi, R.; Mennucci, B.; Pomelli, C.; Adamo, C.; Clifford, S.; Ochterski, J.; Petersson, G. A.; Ayala, P. Y.; Cui, Q.; Morokuma, K.; Malick, D. K.; Rabuck, A. D.; Raghavachari, K.; Foresman, J. B.; Cioslowski, J.; Ortiz, J. V.; Stefanov, B. B.; Liu, G.; Liashenko, A.; Piskorz, P.; Komaromi, I.; Gomperts, R.; Martin, R. L.; Fox, D. J.; Keith, T.; Al-Laham, M. A.; Peng, C. Y.; Nanayakkara, A.; Gonzalez, C.; Challacombe, M.; Gill, P. M. W.; Johnson, B. G.; Chen, W.; Wong, M. W.; Andres, J. L.; Head-Gordon, M.; Replogle, E. S.; Pople, J. A. *Gaussian 98*, revision D.3; Gaussian, Inc.: Pittsburgh, PA, 1998.

(21) Becke, A. D. *J. Chem. Phys.* **1993**, *98*, 5648. Lee, C.; Yang, W.; Parr, R. G. *Phys. Rev. B* **1988**, *37*, 785.

(22) Head-Gordon, M.; Pople, J. A.; Frisch, M. J. *Chem. Phys. Lett*. **1988**, *153*, 503.

(23) Pople, J. A.; Head-Gordon, M.; Raghavachari, K. *J. Chem. Phys.* **1987**, *87*, 5968.

(24) Applying the basis set correction of −2.44 kcal/mol, which reflects the difference between the cc-pVDZ and cc-pVQZ values, yields an effective CCSD(T)/cc-pVQZ value of 6.78 kcal/mol for pathway 1b.

(25) Holbrook, K. A.; Pilling, M. J.; Robertson, S. H. *Unimolecular Reactions*, 2nd ed.; John Wiley & Sons: New York, 1996. Forst, W. *Theory of Unimolecular Reactions*; Academic Press: New York, 1973.

(26) Beyer, T.; Swinehart, D. R. *ACM Commun.* **1973**, *16*, 379

(27) Olzmann, M.; Kraka, E.; Cremer, D.; Gutbrod, R.; Andersson, S. *J. Phys. Chem. A* **1997**, *101*, 9421.

(28) Troe, J. *J. Phys. Chem*. **1979**, *83*, 114.

(29) Barker, J. R.; Golden, R. E. *J. Phys. Chem*. **1984**, *88*, 1012.

(30) Shi, J.; Barker, J. R. *J. Chem. Phys*. **1988**, *88*, 6219.

(31) Oref, I.; Tardy, D. C. *Chem. Rev*. **1990**, *90*, 1407.

(32) Barker, J. R. Multiwell-1.3.1 software, 2003. Barker, J. R. *Int. J. Chem. Kinet.* **2001**, *33*, 232.

(33) Gilbert, R G.; Smith S. C. *Theory of Unimolecular and Recombination Reactions*; Blackwell: Oxford, 1990.

(34) Troe, J. *J. Chem. Phys.* **1977**, *66*, 4745.

(35) DeMore, W. B.; Sander, S. P.; Golden, D. M.; Hampson, R. F.; Kurylo, M. J.; Howard, C. J.; Ravishankara, A. R.; Kolb, C. E.; Molina, M. J. *Chemical kinetics and photochemical data for use in stratospheric modeling*. JPL Publication 92; NASA Jet Propulsion Laboratory: Pasadena, CA, 1992.

(36) Dibble, T. S. *J. Phys. Chem. A.* **2002**, *106*, 6643.

(37) Lei, W.; Zhang, R.; McGivern, W. S.; Derecskei-Kovas, A.; North, S. W. *J. Phys. Chem. A* **2001**, *105*, 471.

(38) McGivern, W. S.; Suh, I.; Clinkenbeard, A. D.; Zhang, R.; North, S. W. *J. Phys. Chem. A* **2000**, *104*, 6609.

(39) Atkinson, R. *Int. J. Chem. Kinet*. **1997**, *29*, 99.

(40) Zhao, J.; Zhang R.; North, S. W. *Chem. Phys. Lett*. **2003**, *369*, 204.

(41) Orlando, J. J.; Tyndall, G. S.; Bilde, M.; Ferronato, C.; Wallington, T. J.; Vereecken, L.; Peeters, J. *J. Phys. Chem. A* **1998**, *102*, 8116.

(42) Schneider, W. F.; Wallington, T. J.; Barker, J. R.; Stahlberg, E. A. *Ber. Bunsen-Ges. Phys. Chem*. **1998**, *102*, 1850.

(43) Vereecken, L.; Huyberechts, G.; Peeters, J. *J. Chem. Phys.* **1997**, *106*, 6564.

(44) Vereecken, L.; Peeters, J. *J. Phys. Chem. A* **1999**, *103*, 1768.

(45) Vereecken, L.; Peeters, J.; Orlando, J. J.; Tyndall, G. S.; Ferronato, C. *J. Phys. Chem. A* **1999**, *103*, 4693.

(46) Atkinson, R. *J. Phys. Chem. Ref. Data* **1997**, *26*, 215.

(47) Miyoshi, A.; Matsui, H.; Washida, N. *J. Phys. Chem*. **1990**, *94*, 3016.